ACS Photonics

Article

pubs.acs.org/journal/apchd5

Localized Surface Plasmon Decay Pathways in Disordered Two-Dimensional Nanoparticle Arrays

Tomasz J. Antosiewicz*,†,‡ and Tomasz Tarkowski§

†Centre of New Technologies, University of Warsaw, Banacha 2c, 02-097 Warsaw, Poland

‡Chalmers University of Technology, Department of Applied Physics, SE-412 96 Göteborg, Sweden

§University of Warsaw, Faculty of Physics, Pasteura 5, 02-093 Warsaw, Poland

ABSTRACT: The size and shape of a metal nanoparticle determine its optical properties. When placed in an array the single particle response is further modified by the scattered fields, which for a random array are unique to each scatterer. However, at the array level scattering and absorption retain single-particle-like spectra. Using T-Matrix calculations and an analytical model of intra-array coupling in amorphous arrays we show how the branching ratio of the localized plasmon decay depends on disorder and particle density. We calculate the effective polarizability and demonstrate its effects on scattering and absorption. The scattering-to-absorption ratio is a function of particle separation in the disordered array and can significantly deviate from the inherent single particle ratio. We trace the period of this oscillatory dependence of the ratio to the single particle plasmon resonance wavelength. This effect has implications for applications in which one of the decay channels has to be dominant, for example, absorption for hot electron−hole pair generation in the metal particles or scattering into a nearby semiconductor.

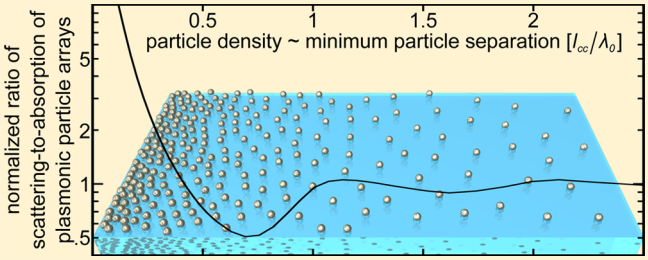

KEYWORDS: *localized surface plasmon, amorphous arrays, disorder, scattering, absorption, nanoparticles, T-Matrix calculations*

Optical properties of materials, whether they are composed of atoms or macroscopic structures, are determined not only by how light interacts with this basic element which makes up the material, but also by how these elements are arranged.[1,2] The latter is often more important, both in transitions from atoms to corresponding solids as well as from nanoparticles to arrays and metamaterials.[3−5] In the macroscopic regime, one could start with a nanostructure that interacts strongly with light and build around it, for example, repeating it periodically. One may choose between dielectrics,[6] semiconductors,[7,8] and metals.[9,10] The appeal of using metals is that they enable excitation of surface plasmons, which due to enhanced near-fields and subwavelength confinement have found their way into a large number of applications including biosensing,[11−13] waveguiding,[14,15] light absorption,[16,17] and plasmon-assisted photocatalysis.[18,19]

The benefit of considering periodic structures is that they are relatively easy to study analytically and/or numerically due to the existence of a unit cell. However, the periodicity may require very accurate, usually top-down, methods to ensure the fabricated structures behave as designed, as the appearance of disorder suppresses, partially or fully, features arising from periodicity.[20−22] A competing alternative to periodic structures are random ones, which can be fabricated by self-assembly methods such as colloidal lithography[23,24] or other techniques.[25] However, periodic arrangements of nanoparticles can be equally well assembled using colloidal techniques.[23]

Elucidation of light−matter interactions in disordered metamaterials,[26] as with periodic, begins with understanding the optical properties of the elementary building block. However, a key difference results from interactions within the array, which ideally are accounted for by an interaction term that modifies the single particle response.[27−29] Unlike a periodic structure, at the nanoscale, the neighborhood of each meta-atom in a random array is unique, implying that the response of any given element is quantitatively different. Yet, at the same time the bulk properties (of the array) are well-defined and qualitatively similar to those of a single, uncoupled meta-atom. This is because the statistical neighborhood of each scatterer is strictly determined by the pair correlation function (PCF). For the dipolar resonance one writes that the effective polarizability[20,27,28] is

$$\alpha^* = \frac{1}{\alpha^{-1} - S} \text{ with } S \propto \int A(r)\rho(r)\mathrm{d}r \tag{1}$$

where α is the single particle polarizability (quasistatic or corrected for radiation and depolarization[30]) and S is an interaction term dependent on dipolar radiation $A(r)$ and the structure factor $\rho(r)$, in the considered case, the PCF.

The optical properties of the structure are uniquely determined by the polarizability. In the quasistatic approximation absorption $\sigma_a \propto \mathrm{Im}(\alpha^*)$, while scattering $\sigma_s \propto |\alpha^*|^2$.

Received: July 28, 2015
Published: November 11, 2015

DOI: 10.1021/acsphotonics.5b00420
ACS Photonics 2015, 2, 1732−1738

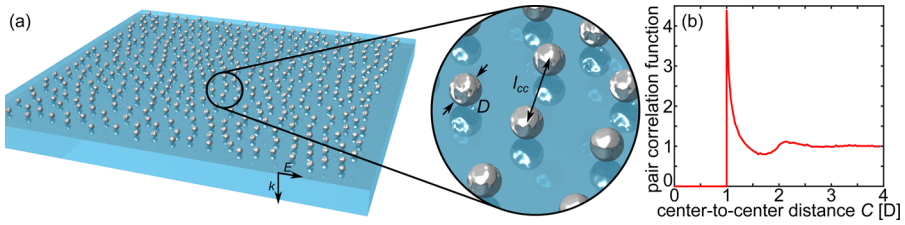

Figure 1. (a) Amorphous (random with short-range order) array of silver nanospheres with diameters D. The separation between all pairs of spheres is larger than the minimum center-to-center distance $l_{cc} = DC$. (b) Pair correlation function for a 2D amorphous array obtained from the random arrays used in T-Matrix calculations.

This means that the interaction term S affects scattering and absorption differently, giving an extra way to modify the ratio of the two decay channels. Such control can then be used to, for example, maximize either of the pathways via which plasmons harvest solar energy: generating hot electron−hole pairs inside the metal (absorption)[19,31] or enhancing the electric fields outside in a surrounding semiconductor (scattering).[17] In this work we demonstrate such control using silver nanospheres, however, this applies equally to other nanoelements with a dominating dipolar response or could be extended to include dipole−quadrupole interactions as well. We should also mention that, while not considered here, the methodology (model and T-Matrix method)[29,32] can also be used to investigate both 1D and 3D amorphous structures.

NUMERICAL CALCULATIONS

To calculate the optical cross sections of the investigated arrays of nanospheres we use the T-Matrix method.[32,33] In this method, the electromagnetic field scattered by N spheres is decomposed into a sum of individual scattered fields. Each sphere is illuminated by an incident (here, a linearly polarized plane wave at normal or oblique incidence) as well as scattered fields of all other particles. The addition theorem for spherical harmonics is used to write the fields scattered by one sphere in terms of spherical harmonics centered about another sphere. Finally, a transformation into a cluster-centered T-Matrix allows for calculation of the optical properties of an investigated structure. In the T-Matrix calculations performed here we include the first four spherical harmonics, which is enough considering only the dipolar and quadrupolar modes are visible.

Two-dimensional arrays of nanospheres with diameters between 20 and 100 nm, a schematic example being shown in Figure 1a, are created using random sequential adsorption (RSA).[34] Briefly, spheres are sequentially, randomly and iteratively added to a surface under a condition that the separation between each pair $l_{cc} = DC$ is not smaller than a minimum value defined by the diameter D and the dimensionless minimum center-to-center (cc) distance C. This mimics random arrays obtained using hole mask colloidal lithography[24] in which electrostatic repulsion between polystyrene nanobeads assures such separation. D and C determine the surface density of particles which is $\sigma = 0.694 l_{cc}^{-2}$ (this prefactor is unique for this type of randomness and here was calculated as a fitting parameter; in general, it is a surface packing parameter). The dimensions of the surface determine the approximate maximum number of particles that can fit, in this case 2100. This is enough to ensure adequate averaging of interparticle interactions and a well-defined plasmon resonance.[29] The permittivity of the particles is described by a Drude function $\epsilon(\omega) = 3.7 - \omega_p^2/(\omega^2 + i\gamma\omega)$, with $\hbar\omega_p = 8.56$ eV and $\hbar\gamma = 66$ meV ($\omega_p/\gamma = 130$) to mimic silver. An array constructed using RSA while random over long distances, exhibits short-range correlation. This is demonstrated by its PCF, which is needed for analytical calculations of their optical properties.[28,29] The 2D PCF calculated directly from amorphous arrays generated by RSA for T-Matrix calculations is plotted in Figure 1b.

SINGLE SPHERES

The focus of this work is on amorphous arrays of plasmonic spheres, however, to set the background first we briefly recall the optical properties of metal spheres, which are summarized in Figure 2. For small spheres made of a material with

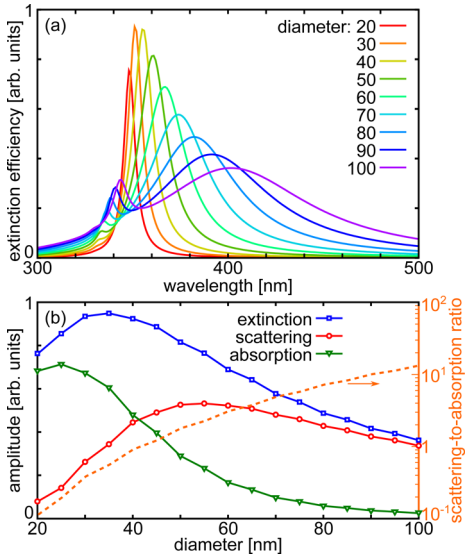

Figure 2. (a) Normalized extinction efficiencies for single spheres with diameters D from 20 to 100 nm. The dipolar, and for large spheres quadrupolar, resonances are visible, becoming weaker and broader as D increases. (b) Amplitudes of the cross section efficiencies at the dipolar resonance (left vertical axis) as a function of D. The single particle scattering-to-absorption ratio is plotted with the dashed line (right vertical axis).

permittivity ϵ the dipolar resonance occurs when $\epsilon = -2\epsilon_s$, where ϵ_s characterizes the surrounding medium. With increasing D the quasistatic approximation ceases to be applicable and radiation and depolarization become important,[30] leading to a red shift of the dipolar resonance which broadens and decreases in amplitude (Figure 2a).

The increase of D affects scattering and absorption differently.[35] Figure 2b shows the dominance of absorption at small D and that at $D \approx 40$ nm scattering becomes larger. In the considered diameter range the single particle scattering-to-absorption ratio $R_{s/a}^{(1)} = \sigma_s/\sigma_a$ changes by 2 orders of magnitude

DOI: 10.1021/acsphotonics.5b00420
ACS Photonics 2015, 2, 1732−1738

proportionally to $\sim D^3$, as it should be. Hence, an individual nanooptical element can be tuned to either scatter or absorb strongly, respectively, being large or small compared to the wavelength. This consignment of scattering/absorption to large/small particles may sometimes be a hindrance, when size limits dictate that only small particles can be used, but should predominantly scatter. For example, such conditions arise in plasmonic solar cells when absorption in the small metal particles is a parasitic effect that lowers overall performance.[36] On the other hand, if the absorption channel is of relevance, for example, for hot electron−hole pair generation in plasmon enhanced catalysis, scattering is detrimental. It may of course be possible to design complex nanostructures with nontrivial responses, for example, Fano resonances to tailor the absorptive/scattering properties and then decorate a substrate with them.[37] However, such complex nanostructures may not be feasible to be produced in large quantities. Thus, it is beneficial to consider if and how disorder can be utilized to control absorption and scattering. Here, we demonstrate this using as an example amorphous 2-dimensional arrays of simple particles with a dominant dipolar response.

DIPOLAR RESONANCE OF DISORDERED ARRAYS

Figure 3 gives an overview of the optical properties of amorphous arrays of nanospheres 60 nm in diameter, chosen as an examplary case. Scattering and absorption spectra for arrays with C from 2 to 10 are shown in Figure 3a and b, respectively, with the curves offset by a constant to avoid overlap. The dipolar plasmon resonance of the arrays oscillates around the single sphere peak at 367 nm with the position and width of scattering and absorption approximately equal. However, the amplitude of the two varies differently with C, as shown in Figure 3c. Scattering exhibits a more uniform value with its amplitude varying less than absorption. The latter is more sensitive to the particle density and has a clear maximum around $C \approx 4$. This local maximum is thus the cause of a minimum of the scattering-to-absorption ratio $R_{s/a}$ at that minimum center-to-center distance, as shown in Figure 3d. The single particle ratio $R^{(1)}_{s/a}$ (dashed line) for D = 60 nm is about 3.2; however, in the investigated arrays, coupling within them changes the ratio from 1.5 to 4, depending on C (note that the number of particles within the array is constant for each C).

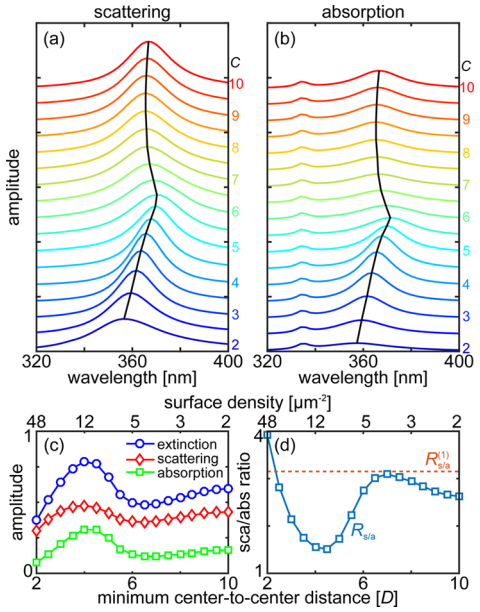

Figure 3. Optical properties of amorphous arrays of nanospheres D = 60 nm with increasing minimum center-to-center distance C. (a) Scattering and (b) absorption show similar behavior of the plasmon resonance which oscillates around the single particle position; the curves are offset by the same value. (c) The amplitude of scattering (diamonds) and absorption (squares) depends differently on C (here in units of D) and (d) their ratio $R_{s/a}$ (squares) oscillates below the single particle value (dashed line).

The possibility of tuning the scattering and absorption decay channels using only the minimum center-to-center distance in an amorphous array opens up an exciting possibility of tailoring the optical activity of virtually any nanostructure. To explore this further we calculate the optical cross sections of arrays made of spheres between 20 and 100 nm, which are typical sizes used in plasmonics. Figure 4a compares the absolute scattering-to-absorption ratios of the investigated arrays (solid lines) to those of the single spheres (horizontal dashed lines) which comprise the arrays. The dependencies of $R_{s/a}$ on C in the displayed cases are qualitatively similar. For dense arrays (and small D) $R_{s/a} > 1$. As the particle density decreases the ratio also decreases until it reaches a minimum, then increases up to the single particle value. Subsequent oscillations are shallower and $R_{s/a}$ remains below the single particle ratio. The position in C of the global minimum and the period of these oscillations decrease for larger sphere sizes.

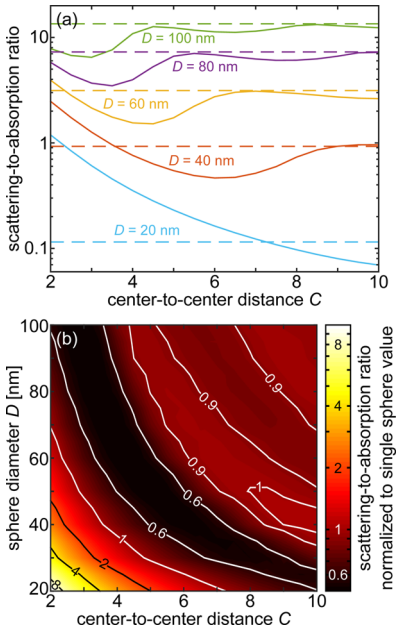

Figure 4. Scattering-to-absorption ratio of amorphous arrays. (a) Absolute ratio for chosen nanosphere diameters: solid line, arrays; dashed line, single sphere. Except for dense arrays of small nanoparticles the ratio is smaller than for single particles. A global minimum is present for values of C that depend inversely on the particle diameter. (b) Scattering-to-absorption ratio $R_{s/a}$ normalized to corresponding single particle ratio. The colorscale and coutour lines indicate the fraction of the single particle scattering-to-absorption ratio exhibited by arrays of those particles.

The similarity between $R_{s/a}$ for all diameters is shown clearly in Figure 4b. There we plot scattering-to-absorption ratios of random arrays normalized to the single particle values. In essence, this plot shows by how much the single particle $R_{s/a}$

DOI: 10.1021/acsphotonics.5b00420
ACS Photonics 2015, 2, 1732−1738

changes when subject to the scattered fields of other nanospheres. The most striking feature is the minimum of about 0.5, a value which is almost constant for all considered D. For dense arrays the dominant trend is an increase of the ratio, for example, nanospheres with D = 20 nm exhibit an almost 1 order of magnitude increase of $R_{s/a}$ at C = 2 (so that $\sigma_s \approx \sigma_a$, namely, Figure 4a). For larger D the increase is smaller as the global minimum starts to dominate at increasingly smaller C. To explore in detail the origins of this behavior, we investigate the scattered fields of these arrays.

INFLUENCE OF THE SCATTERED FIELDS

The observed changes of the branching ratio of plasmon damping into Joule heating and scattering are caused by the interaction between the nanospheres in the arrays. As noted in the introduction, the influence of the reradiated fields is contained within the interaction term S. To arrive at an expression which correctly describes stochastic scattering of a random array one needs to assume that the global properties of a random array are described properly by those of an average particle.[28,29] This way all the particles are equal and are subject to the same self-consistently calculated fields. The effect of these fields is then incorporated into an effective polarizability $\alpha^* = (\alpha^{-1} - S)^{-1}$. In a qualitative manner, dropping prefactors and retaining the quasistatic approximation, we write

$$\sigma_a \propto \mathrm{Im}\left[\frac{\alpha}{1-\alpha S}\right] = \frac{\mathrm{Im}[\alpha] + |\alpha|^2 \mathrm{Im}[S]}{|1-\alpha S|^2}$$

and

$$\sigma_s \propto \frac{|\alpha|^2}{|1-\alpha S|^2} \qquad (2a,b)$$

for absorption and scattering, respectively. One immediately notices that both σ_a and σ_s have a common denominator that depends on S, but, critically, absorption also depends on S in the numerator. The single nanosphere scattering-to-absorption ratio $R_{s/a}$ is proportional to $|\alpha|^2(\mathrm{Im}[\alpha])^{-1}$, hence increases proportionally to particle volume. A nonzero S modifies this ratio to

$$\frac{1}{R_{s/a}} \propto \frac{\mathrm{Im}[\alpha]}{|\alpha|^2} + \mathrm{Im}[S] \qquad (3)$$

This shows explicitly that the interaction modifies the branching ratio proportionally to the imaginary part of the interaction field. As introduced in eq 1, S depends on the dipole radiation and the structure factor. The structure factor's main feature is a Heaviside step function $\Theta(r - l_{cc})$ with corrections near the l_{cc} cutoff, see Figure 1b. A qualitative analysis of S using only the dominating Heaviside part[28] gives

$$S_\Theta = \pi\sigma\frac{e^{ikl_{cc}}}{l_{cc}}(1 + ikl_{cc}) \qquad (4)$$

where $k = 2\pi/\lambda$ is the wavenumber and λ the wavelength. In the limit of very sparse arrays $\lim_{l_{cc}\to\infty} S_\Theta = 0$, which restores the single particle properties. As the particle density increases, so does S_Θ, however, due to the exponential term, the real and imaginary parts oscillate between positive and negative. As reported before,[28,29] the real part is responsible for oscillations of the peak position. Here, we focus on the imaginary part, which dictates the splitting ratio between scattering and absorption. Substituting eq 4 into eq 3 yields

$$\frac{1}{R_{s/a}} \propto \frac{\mathrm{Im}[\alpha]}{|\alpha|^2} + \frac{\pi\sigma}{l_{cc}}(kl_{cc}\cos kl_{cc} + \sin kl_{cc}) \qquad (5)$$

showing explicitly the origin of the oscillations of the scattering-to-absorption ratio with a varying l_{cc}. It also explains why arrays made of larger particles exhibit a shorter period of the oscillations of $R_{s/a}$, as shown in Figure 4, the reason being the kl_{cc} argument in the exponent. The simplicity of eq 5 is evident when we plot the normalized scattering-to-absorption ratio versus the minimum center-to-center distance expressed in units of the single particle plasmon wavelength λ_0. Plotted in Figure 5, all the lines basically collapse back to one in

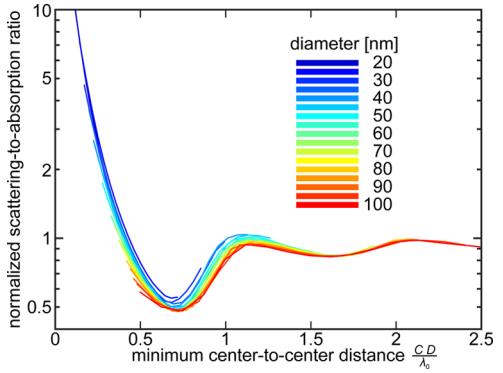

Figure 5. Scattering-to-absorption ratio of amorphous arrays normalized to their respective single particle values plotted versus the distance between the nearest neighbors normalized to the single particle resonance wavelength CD/λ_0. Note that all lines basically collapse back to one with slight dispersion, highlighting the universal dependence of the scattering-to-absorption ratio on the minimum cc distance and the phase of the interaction fields arriving at a particle in relation to the source.

agreement with a universal scaling of the interaction term S. The dependence of the oscillations on l_{cc}/λ_0 means that the important factor is the phase difference between the scattered fields and the source at the particle.

An interesting observation is that the contribution from S, and consequently the modification of the single particle response, is larger for smaller nanoparticles as a function of C (cf. Figure 4). This may be slightly counterintuitive, since S depends on the interaction fields which are proportional to the scattering efficiency of a particle. However, one has to keep in mind that with a shrinking diameter the physical separation l_{cc} between nanoparticles also decreases. Hence, even though scattering decreases (with D), the near-field interaction compensates for the loss in radiation efficiency.

As the final point we investigate how the scattering-to-absorption ratio depends on the angle of incidence α and polarization, with results shown in Figure 6 for D = 40 nm. For s-polarized light (Figure 6a) the change brought about by a shallower incidence angle is relatively quick; already at $\alpha = 0.2\pi$ the deep minimum of $R_{s/a}$ disappears and at larger angles the $R_{s/a}$ becomes an almost monotonously decreasing function of C. At large angles of incidence, p-polarized light (Figure 6b) causes similar effects as s-polarized, however, the ratio is smaller, for example, the red lines for 0.4π. At small α the ratio is similar to that under normal incidence, but the variations of the ratio are smaller than for $\alpha = 0$.

There are two causes of this behavior. The first is that depending on the polarization, each particle couples efficiently

DOI: 10.1021/acsphotonics.5b00420
ACS Photonics 2015, 2, 1732−1738

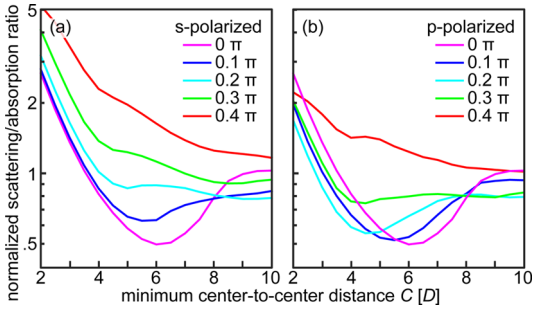

Figure 6. Normalized scattering-to-absorption ratio of amorphous arrays illuminated at oblique incidence (from 0 to 0.4π) for (a) *s*- and (b) *p*-polarized light. For *s*-polarized light, the ratio increases 2-fold for dense arrays and the minimum disappears. At small angles of incidence for *p*-polarization the ratio changes little; the variations become smaller than for normal incidence; only at large angles the minimum disappears, but the amplitude is smaller than for *s*-polarization.

with a different number of its neighbors. For *s*-polarized light the electric field is always in the plane of the array. Thus, due to the nature of dipolar radiation each particle interacts strongly only with those lying in its symmetry plane. However, for *p*-polarized light as α increases the particles are excited with an increasingly stronger out-of-(array)-plane component. The normally oriented resonance couples efficiently with all particles (neglecting the inverse radial dependence) because the radiation maximum is directed in the plane of the array. Thus, the interaction parameter S is larger for *p*-polarized light and causes the changes of $R_{s/a}$ to be larger for this polarization. Furthermore, at small α the out-of-plane component of *s*-polarized light is small, so the deviations from normal incidence properties are minor. The second reason is that under oblique incidence the resonances in particles are excited with a phase shift that increases with α. This causes scattered fields from opposite sides to arrive at any given particle increasingly out-of-phase; in the coupled model this implies that it is no longer possible to obtain perfect constructive and destructive interference, that is, a lack of clear maxima and minima of $R_{s/a}$. These results indicate that the enhancement of scattering is present in all considered cases for dense arrays at any angle of incidence. However, to enhance absorption it is necessary to ensure close to normal incidence of light, requiring solar tracking to orient the planar device appropriately to harvest sunlight.

CONCLUSIONS AND SUMMARY

The scattered fields that ensure electromagnetic self-consistency within an array are an important source affecting the optical properties of materials. Commonly used for establishing narrow resonances via diffraction, they are equally critical for understanding how random and quasi-random structures interact with light.[26] Using analytical calculations and results obtained by the T-Matrix method we have shown how interactions in disordered materials affect the optical properties of single elements. Specifically, we have focused on the scattering-to-absorption ratio, which is a key parameter determining how an array of nanostructures dispersed amorphously on a surface can be used.

Figures 4 and 5 show the extent of changes of the ratio possible to achieve in amorphous arrays of silver nanospheres depending of the nanoparticle density. The largest effects are, of course, observed for dense arrays for which the interaction fields and, consequently, the interaction term are large. In fact, there is considerable variation of the strength of S already for relatively small changes of the density. The most profound example considered in this work is a 20 nm nanosphere and arrays composed of it. By itself, this plasmonic particle absorbs over 90% of energy directed at it. However, when placed in an amorphous array with a center-to-center distance of 2, the scattering-to-absorption ratio is 1. Scattering, at the expense of absorption, is enhanced by 1 order of magnitude. This is a considerable change which could affect the efficiency of solar harvesting,[38] especially when the nanomaterial properties were designed considering only single particle characteristics. For even smaller diameters the enhancement of scattering is expected to be even greater, however, nonlocal,[39,40] surface spill-out,[41,42] and quantum size effects[40,43,44] are expected to influence the optical properties of such arrays.

As nanoparticles increase in size, the relative changes of the ratio decrease for the same center-to-center distance or, more precisely, shift to even smaller values of C, see Figure 4b. This makes the coupling behavior in random arrays relatively predictable. It is thus entirely possible to tailor a nanoarray to very specific properties. In solar harvesting of paramount importance is the ability to use as much sunlight as possible: these may be enhanced near-fields, increased scattering into a photoactive medium,[17] or greater hot electron−hole pair generation[19,31] in the plasmonic nanostructure. Especially the last two points are mutually exclusive and one generally aims at maximizing one at the expense of the other. This work demonstrates how to achieve this goal in bottom-up fabricated random/amorphous arrays. Using a 40 nm sphere as an example, we note that it has an inherent $R_{s/a} \approx 1$. A dense array with $C = 2$ promotes scattering with a ratio of 3. On the other hand, using a 9 times lower density ($C = 6$) results in scattering being 0.6 of absorption. Including these considerations into designing working nanostructures allows for the most efficient use of a plasmonic material. We should note that here we have considered only monodisperse nanoparticle distributions,[45] however, in some realizations that is not the case.[46] A size dispersion will vary the resonances of individual spheres, thereby affecting the strength and phase of the interaction fields, leading probably to a weaker dependence on S. The interaction term S is also affected by the incidence angle and polarization, meaning these two factors also influence the branching ratio.

In summary, we have discussed how to account for scattered fields in the optical properties of disordered arrays, whose scattering and absorption spectra can be severely modified with respect to those of the single particle. These modifications, aside from peak position changes, affect also the branching ratio of plasmon decay, making this a relevant study of any applications which use bottom-up fabrication methods that produce disordered arrays. Depending on the size of the constituent element of the array, the scattering-to-absorption ratio can change anywhere from factors of 0.6 up to 10 of the single particle value, favoring applications that employ direct solar harvesting in the plasmonic particle (absorption) or those which use these particles to enhance harvesting in the surrounding medium (scattering). This makes our results important when aiming to maximize the efficiency of a plasmonic composite material or, indeed, any nanophotonic structure composed of disordered resonant particles.

DOI: 10.1021/acsphotonics.5b00420
ACS Photonics 2015, 2, 1732−1738

AUTHOR INFORMATION

Corresponding Author

*E-mail: tomasz.antosiewicz@uw.edu.pl.

Notes

The authors declare no competing financial interest.

ACKNOWLEDGMENTS

This work was supported by the Foundation for Polish Science via the Project HOMING PLUS/2013-7/1 and the Polish Ministry of Science and Higher Education via the Iuventus Plus Project IP2014 000473. Numerical calculations were performed at the ICM at the University of Warsaw, Grant No. G55-6. We thank S. Peter Apell for useful comments on the manuscript.

REFERENCES

(1) Kabashin, A. V.; Evans, P.; Pastkovsky, S.; Hendren, W.; Wurtz, G. A.; Atkinson, R.; Pollard, R.; Podolskiy, V. A.; Zayats, A. V. Plasmonic Nanorod Metamaterials for Biosensing. *Nat. Mater.* **2009**, *8*, 867−871.

(2) Humphrey, A. D.; Barnes, W. L. Plasmonic Surface Lattice Resonances on Arrays of Different Lattice Symmetry. *Phys. Rev. B: Condens. Matter Mater. Phys.* **2014**, *90*, 075404.

(3) Vasilantonakis, N.; Terzaki, K.; Sakellari, I.; Purlys, V.; Gray, D.; Soukoulis, C. M.; Vamvakaki, M.; Kafesaki, M.; Farsari, M. Three-Dimensional Metallic Photonic Crystals with Optical Bandgaps. *Adv. Mater.* **2012**, *24*, 1101−1105.

(4) Chou, J. B.; Yeng, Y. X.; Lenert, A.; Rinnerbauer, V.; Celanovic, I.; Soljačić, M.; Wang, E. N.; Kim, S.-G. Design of Wide-Angle Selective Absorbers/Emitters with Dielectric Filled Metallic Photonic Crystals for Energy Applications. *Opt. Express* **2014**, *22*, A144−A154.

(5) Bauer, C.; Giessen, H. Optical Properties of Aperiodic Metallic Photonic Crystal Structures: Quasicrystals and Disorder. *J. Opt.* **2014**, *16*, 114001.

(6) Schroden, R. C.; Al-Daous, M.; Blanford, C. F.; Stein, A. Optical Properties of Inverse Opal Photonic Crystals. *Chem. Mater.* **2002**, *14*, 3305−3315.

(7) Kepińska, M.; Starczewska, A.; Bednarczyk, I.; Szala, J.; Szperlich, P.; Mistewicz, K. Fabrication and Characterisation of SbI_3-Opal Structures. *Mater. Lett.* **2014**, *130*, 17−20.

(8) Karuturi, S. K.; Cheng, C.; Liu, L.; Su, L. T.; Fan, H. J.; Tok, A. I. Y. Inverse Opals Coupled with Nanowires as Photoelectrochemical Anode. *Nano Energy* **2012**, *1*, 322−327.

(9) Czaplicki, R.; Husu, H.; Siikanen, R.; Mäkitalo, J.; Kauranen, M.; Laukkanen, J.; Lehtolahti, J.; Kuittinen, M. Enhancement of Second-Harmonic Generation from Metal Nanoparticles by Passive Elements. *Phys. Rev. Lett.* **2013**, *110*, 093902.

(10) Spinelli, P.; Hebbink, M.; de Waele, R.; Black, L.; Lenzmann, F.; Polman, A. Optical Impedance Matching Using Coupled Plasmonic Nanoparticle Arrays. *Nano Lett.* **2011**, *11*, 1760−1765.

(11) Antosiewicz, T. J.; Apell, S. P.; Claudio, V.; Käll, M. A Simple Model for the Resonance Shift of Localized Plasmons Due to Dielectric Particle Adhesion. *Opt. Express* **2012**, *20*, 524−533.

(12) Beuwer, M. A.; Prins, M. W. J.; Zijlstra, P. Stochastic Protein Interactions Monitored by Hundreds of Single-Molecule Plasmonic Biosensors. *Nano Lett.* **2015**, *15*, 3507−3511.

(13) Rodrigo, D.; Limaj, O.; Janner, D.; Etezadi, D.; García de Abajo, F. J.; Pruneri, V.; Altug, H. Mid-Infrared Plasmonic Biosensing with Graphene. *Science* **2015**, *349*, 165−168.

(14) Saj, W. M.; Antosiewicz, T. J.; Pniewski, J.; Szoplik, T. Energy Transport in Plasmon Waveguides on Chain of Metal Nanoplates. *Opto-Electron. Rev.* **2006**, *14*, 243−251.

(15) Ahmadivand, A.; Golmohammadi, S. Compositional Arrangement of Rod/Shell Nanoparticles: An Approach to Provide Efficient Plasmon Waveguides. *Opto-Electron. Rev.* **2014**, *22*, 101−108.

(16) Antosiewicz, T. J.; Apell, S. P.; Wadell, C.; Langhammer, C. Absorption Enhancement in Lossy Transition Metal Elements of Plasmonic Nanosandwiches. *J. Phys. Chem. C* **2012**, *116*, 20522−20529.

(17) Lee, D. H.; Kwon, J. Y.; Maldonado, S.; Tuteja, A.; Boukai, A. Extreme Light Absorption by Multiple Plasmonic Layers on Upgraded Metallurgical Grade Silicon Solar Cells. *Nano Lett.* **2014**, *14*, 1961−1967.

(18) Clavero, C. Plasmon-Induced Hot-Electron Generation at Nanoparticle/Metal-Oxide Interfaces for Photovoltaic and Photocatalytic Devices. *Nat. Photonics* **2014**, *8*, 95−103.

(19) Kale, M. J.; Avanesian, T.; Christopher, P. Direct Photocatalysis by Plasmonic Nanostructures. *ACS Catal.* **2014**, *4*, 116−128.

(20) Auguié, B.; Barnes, W. L. Diffractive Coupling in Gold Nanoparticle Arrays and the Effect of Disorder. *Opt. Lett.* **2009**, *34*, 401−403.

(21) Andueza, A.; Smet, T.; Morales, P.; Sevilla, J. Disorder Effect in the Transmission Spectra of a Noncompact Single Layer of Dielectric Spheres Derived from Microwave Spectroscopy. *Appl. Opt.* **2011**, *50*, G91−G97.

(22) Natarov, D. M.; Marciniak, M.; Sauleau, R.; Nosich, A. I. Seeing the Order in a Mess: Optical Signature of Periodicity in a Cloud of Plasmonic Nanowires. *Opt. Express* **2014**, *22*, 28190−8198.

(23) Yang, S.-M.; Jang, S. G.; Choi, D.-G.; Kim, S.; Yu, H. K. Nanomachining by Colloidal Lithography. *Small* **2006**, *2*, 458−475.

(24) Fredriksson, H.; Alaverdyan, Y.; Dmitriev, A.; Langhammer, C.; Sutherland, D. S.; Zäch, M.; Kasemo, B. Hole-Mask Coloidal Lithography. *Adv. Mater.* **2007**, *19*, 4297−4302.

(25) Prikulis, J.; Malinovskis, U.; Poplausks, R.; Apsite, I.; Bergs, G.; Erts, D. Optical Scattering by Dense Disordered Metal Nanoparticle Arrays. *Plasmonics* **2014**, *9*, 427−434.

(26) Albooyeh, M.; Kruk, S.; Menzel, C.; Helgert, C.; Kroll, M.; Krysinski, A.; Decker, M.; Neshev, D. N.; Pertsch, T.; Etrich, C.; Rockstuhl, C.; Tretyakov, S. A.; Simovski, C. R.; Kivshar, Y. S. Resonant Metasurfaces at Oblique Incidence: Interplay of Order and Disorder. *Sci. Rep.* **2014**, *4*, 4484.

(27) Przybilla, F.; Genet, C.; Ebbesen, T. W. Long vs. Short-Range Orders in Random Subwavelength Hole Arrays. *Opt. Express* **2012**, *20*, 4697−4709.

(28) Antosiewicz, T. J.; Apell, S. P.; Zäch, M.; Zorić, I.; Langhammer, C. Oscillatory Optical Response of an Amorphous Two-Dimensional Array of Gold Nanoparticles. *Phys. Rev. Lett.* **2012**, *109*, 247401.

(29) Antosiewicz, T. J.; Apell, S. P. Plasmonic Glasses: Optical Properties of Amorphous Metal-Dielectric Composites. *Opt. Express* **2014**, *22*, 2031−2042.

(30) Moroz, A. Depolarization Field of Spheroidal Particles. *J. Opt. Soc. Am. B* **2009**, *26*, 517−527.

(31) Brongersma, M. L.; Halas, N. J.; Nordlander, P. Plasmon-Induced Hot Carrier Science and Technology. *Nat. Nanotechnol.* **2015**, *10*, 25−34.

(32) Mackowski, D. W. Calculation of Total Cross Section of Multiple-Sphere Clusters. *J. Opt. Soc. Am. A* **1994**, *11*, 2851−2861.

(33) http://www.eng.auburn.edu/users/dmckwski/scatcodes/.

(34) Hinrichsen, E. L.; Feder, J.; Jøssang, T. Geometry of Random Sequential Adsorption. *J. Stat. Phys.* **1986**, *44*, 793−827.

(35) Bohren, C.; Huffman, D. *Absorption and Scattering of Light by Small Particles*; John Wiley and Sons, Inc.: New York, 1983.

(36) Spinelli, P.; Polman, A. Prospects of Near-Field Plasmonic Absorption Enhancement in Semiconductor Materials Using Embedded Ag Nanoparticles. *Opt. Express* **2012**, *20*, A641−A654.

(37) Kang, M.; Chong, Y. D.; Wang, H.-T.; Zhu, W.; Premaratne, M. Critical Route for Coherent Perfect Absorption in a Fano Resonance Plasmonic System. *Appl. Phys. Lett.* **2014**, *105*, 131103.

(38) Sarina, S.; Zhu, H.-Y.; Xiao, Q.; Jaatinen, E.; Jia, J.; Huang, Y.; Zheng, Z.; Wu, H. Viable Photocatalysts Under Solar-Spectrum Irradiation: Nonplasmonic Metal Nanoparticles. *Angew. Chem., Int. Ed.* **2014**, *53*, 2935−2940.

(39) Christensen, T.; Yan, W.; Raza, S.; Jauho, A.-P.; Mortensen, N. A.; Wubs, M. Nonlocal Response of Metallic Nanospheres Probed by Light, Electrons, and Atoms. *ACS Nano* **2014**, *8*, 1745−1758.

DOI: 10.1021/acsphotonics.5b00420
ACS Photonics 2015, 2, 1732−1738

(40) Teperik, T. V.; Nordlander, P.; Aizpurua, J.; Borisov, A. G. Quantum Effects and Nonlocality in Strongly Coupled Plasmonic Nanowire Dimers. *Opt. Express* **2013**, *21*, 27306−27325.
(41) Monreal, R. C.; Apell, S. P.; Antosiewicz, T. J. Surface Scattering Contribution to the Plasmon Width in Embedded Ag Nanospheres. *Opt. Express* **2014**, *22*, 24994−25004.
(42) Monreal, R. C.; Antosiewicz, T. J.; Apell, S. P. Diffuse Surface Scattering in the Plasmonic Resonances of Ultralow Electron Density Nanospheres. *J. Phys. Chem. Lett.* **2015**, *6*, 1847−1853.
(43) Schimpf, A. M.; Thakkar, N.; Gunthardt, C. E.; Masiello, D. J.; Gamelin, D. R. Charge-Tunable Quantum Plasmons in Colloidal Semiconductor Nanocrystals. *ACS Nano* **2014**, *8*, 1065−1072.
(44) Kulkarni, V.; Manjavacas, A. Quantum Effects in Charge Transfer Plasmons. *ACS Photonics* **2015**, *2*, 987−992.
(45) Wettergren, K.; Schweinberger, F. F.; Deiana, D.; Ridge, C. J.; Crampton, A. S.; Rötzer, M. D.; Hansen, T. W.; Zhdanov, V. P.; Heiz, U.; Langhammer, C. High Sintering Resistance of Size-Selected Platinum Cluster Catalysts by Suppressed Ostwald Ripening. *Nano Lett.* **2014**, *14*, 5803−5809.
(46) Knight, M. W.; Coenen, T.; Yang, Y.; Brenny, B. J. M.; Losurdo, M.; Brown, A. S.; Everitt, H. O.; Polman, A. Gallium Plasmonics: Deep Subwavelength Spectroscopic Imaging of Single and Interacting Gallium Nanoparticles. *ACS Nano* **2015**, *9*, 2049−2060.

DOI: 10.1021/acsphotonics.5b00420
ACS Photonics 2015, 2, 1732−1738